First-principles simulations of electrified interfaces in electrochemistry

Stephen E. Weitzner
Lawrence Livermore National Laboratory, Livermore, CA 94551, USA.

Ismaila Dabo
Department of Materials Science and Engineering
The Pennsylvania State University, University Park, PA 16802, USA.

1 Towards stable and high-performance electrocatalysts

Electrochemical catalysts or *electrocatalysts* are used to interconvert electrical and chemical energy in electrochemical cells. This class of catalysts serves as the enabling technology for electrolysis cells, fuel cells, and a variety of electrochemical reactors that can be used to either store electrical energy in the chemical bonds of molecules, or to alternatively produce commodity chemicals via electrochemical reactions. Historically, platinum group metals have been used as the active material in electrochemical cells in light of their intrinsically high catalytic activity for a multitude of chemical and electrochemical reactions. However, the widespread adoption and commercialization of a number of electrochemical cells has been hindered due to the high cost of platinum group metals. A key focus of modern research has been to design new active materials that are either free of expensive platinum group metals or contain negligible amounts of them, while simultaneously developing an understanding of how certain reactions proceed over catalyst surfaces so as to improve the mass activity and selectivity for particular reaction pathways.[1] A number of approaches have been pursued to lower the cost of electrocatalysts, such as the preparation of shape-controlled metal nanoparticles and nanoporous metal foams, both of which boast high specific surface areas, effectively minimizing the amount of active material needed to achieve a threshold mass activity.[2] Through these efforts, it was also discovered that nanostructuring electrocatalysts can lead to further performance improvements through finite size effects that occur as a result of the unique electronic properties of nanoscale metals.[3, 4] Further cost reductions may be realized by alloying the expensive catalytically active components with cheaper coinage metals such as silver and copper, or base metals such as nickel or aluminum. The incorporation of multiple metals can lead to additional performance enhancement by way of ligand, strain, and ensemble effects that arise as a result of the difference in electronic structure of the alloyed metals, atomic size differences, and preferential organization of components within the surface layer.[5, 6, 7] Similarly, performance enhancements may arise through bifunctional effects where different alloy components present along the surface may work cooperatively to enhance the rate of an electrochemical step in a reaction pathway.[8] Each of these effects are generally interrelated, and the extent to which they may be present can be assessed through the combined use of electroanalytical methods such as cyclic voltammetry, scanning probe techniques such as scanning tunneling microscopy, and first principles approaches such as density functional theory. While it has been widely observed that the activity and selectivity of electrocatalysts can be improved through nanostructuring and alloying, an ongoing challenge has been the ability to rationally design high performance electrocatalysts that are additionally stable in corrosive environments and capable of withstanding large applied voltages.[9, 10, 11] As a motivating example, we briefly consider core-shell catalyst architectures, where the active component is present as a thin shell on a cheaper core metal. As shown schematically in Fig. 1, core-shell catalysts may be subject to *metal migration* effects where the catalytically active shell components diffuse into the core of the electrocatalyst, thereby reducing the concentration of active sites along the surface, or may similarly experience *dissolution* effects where catalytically active components dissolve into the surrounding electrolyte, again effectively diluting the number of sites available for electrocatalysis.

Obtaining a detailed understanding of the conditions under which particular electrocatalysts degrade is an

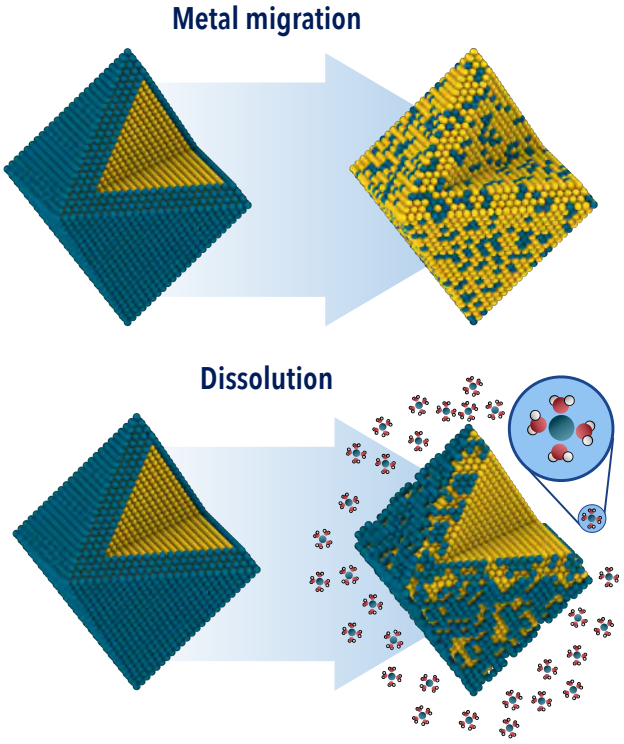

Figure 1: Modern electrocatalysts based on transition metal alloy chemistries can degrade through metal migration and dissolution effects. Mitigation of these and other related degradation mechanisms is a prominent focus of modern research.

important preliminary step to designing scalable and commercially viable electrochemical cells with durable and cost-effective electrocatalysts.

In this chapter, we discuss some of the recent advances made in the first principles modeling of electrochemical catalysts. The key development, as will be discussed, is the ability to explicitly treat the effects of surface electrification due to electrochemical processes and applied voltages in a computationally efficient manner. The latter is achieved using a multiscale quantum-continuum approach that leverages an embedded polarizable continuum model to efficiently treat the electrolyte. We begin the discussion by first introducing the thermodynamics and statistical mechanics of electrified metal-solution interfaces. We subsequently discuss the structure of the electrode-electrolyte interface and the effects of applied voltages. And finally, we conclude with an overview of the first-principles model and a motivating example.

2 A brief thermodynamic detour

Before we proceed to discuss some of the modern developments in the modeling of electrochemical catalysts, it is worthwhile to touch on a few important concepts in chemical thermodynamics and electrochemistry. In the following sections, we provide a brief summary of classical thermodynamics and discuss the thermodynamics of electrified electrode-electrolyte interfaces. The following is by no means intended to provide a full overview of these subjects, but rather to merely provide a basis through which the subsequently developed models can be discussed. We furthermore assume that the reader has had little exposure to thermodynamics prior to reading this text, and therefore present the material at a level suitable for first or second year undergraduates. For a more thorough overview of chemical thermodynamics and statistical mechanics, we highly recommend Refs. [12, 13].

2.1 The fundamental relation

Throughout the study of thermodynamics, we are fundamentally concerned with the flow of energy and matter between a *system* and its *surroundings*. As shown in Fig. 2, we can place certain restrictions on the boundary of our defined system, such that it can be an *open* system so that heat, work, and mass can be freely exchanged with its surroundings, a completely *isolated* system that prevents any type of energy or mass transfer, and several other types of boundaries that selectively allow heat, work, and mass transfer. This notion of boundary permeability to energy transfer is critically important to understand and to define

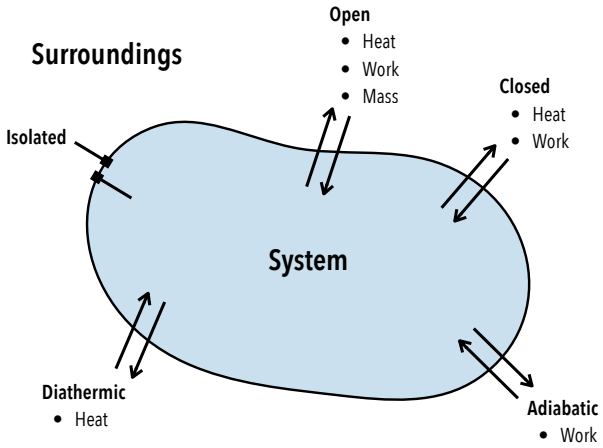

Figure 2: Depending on the type of thermodynamic wall being considered, we can alter how a system interacts with its surroundings. For example, a system with open boundaries allow energy to be exchanged between the system and surroundings in the form of heat, work, and matter, while diathermic boundaries that are rigid and impermeable allow only heat to be exchanged.

since energy and matter are conserved quantities, and can therefore only be transferred or transformed. This is stipulated by the *first law of thermodynamics*, which states that the change in internal energy dU of a system is equal to the amount of heat and work that is exchanged with its surroundings

$$dU = \delta\mathcal{Q} + \delta W, \tag{1}$$

where $\delta\mathcal{Q}$ and δW are infinitesimal amounts of heat and work, respectively.[1] While the first law ensures the conservation of energy, it does not actually place any limits on the exchange of heat or work between a system and its surroundings. Understanding how energy is transferred and defining the rules by which it can transfer is useful since there are a multitude of ways in which the internal energy change dU may be realized.

It is straightforward to first think about what kind of work can be performed on or by a system. We can express the total amount of work as $\delta W = \sum_i \delta W_i$, whose value depends on the types of work δW_i that are possible. One can, for example, consider the *mechanical* work $-PdV$ that is done to compress or expand a volume by an amount dV at a pressure P, the *chemical* work μdN that is done by adding or removing dN atoms or molecules to a system at a chemical potential of μ, and the *electrical* work ΦdQ that is done by adding or removing an electronic charge dQ to the system at a voltage of Φ. In the case that each of these processes are allowed to occur, we can rewrite Eq. 1 as

$$dU = \delta\mathcal{Q} - PdV + \sum_i \mu_i dN_i + \Phi dQ. \tag{2}$$

[1]Here, we differentiate between an exact differential quantity dX and an inexact differential quantity δY such that X is defined to be a state function whose cyclic integral vanishes $\oint dX = 0$, while no such condition is guaranteed for an inexact differential $\oint \delta Y \neq 0$. This is to say, the extent of heat transfer and work done by or to a system are path-dependent or depend on the manner in which the processes are carried out, while the change in a thermodynamic potential such as the internal energy U or entropy S are path-independent, and thus depend only upon the initial and final states of the system.

While the work contributions to the change in internal energy are straightforward to specify, the extent of heat transfer is less obvious and requires a somewhat more in depth discussion. In order to define $\delta\mathcal{Q}$, it is useful to first recall that real processes that are observed to occur in nature such as the mixing of two different gases or heat transfer from hot regions to colder regions occur spontaneously or *irreversibly*. That is, for a given system in an initially non-equilibrium state, the system will tend to evolve towards an equilibrium state in which it will remain until acted upon by some externally applied force. Thus, once a system is at equilibrium with its surroundings, the driving force to move to a different state vanishes. In the context of the examples provided above, gases will continue to mix until their constituent particles are homogeneously distributed creating a spatially uniform composition and heat will continue to transfer until a spatially uniform temperature in the system is achieved. The extent to which a process is considered to be spontaneous or irreversible is characterized by the change in the *entropy* S of the system. Formally, entropy is defined to be a state function and a property of a system similar to the way in which internal energy is a property of a system. The change in entropy can be expressed as

$$dS = \frac{\delta\mathcal{Q}}{T}, \tag{3}$$

where T is the temperature at which the heat transfer is conducted. Physically speaking, Eq. 3 states that the gain in entropy due to a transfer of heat is greater for a system at low temperature than for the same system at an elevated temperature. Furthermore, a system is said to be at equilibrium with its surroundings when the total entropy of the system and surroundings is maximized upon which $dS = 0$. A simple example demonstrating this fact is shown below in Fig. 3. Here, we consider an isolated system that is partitioned

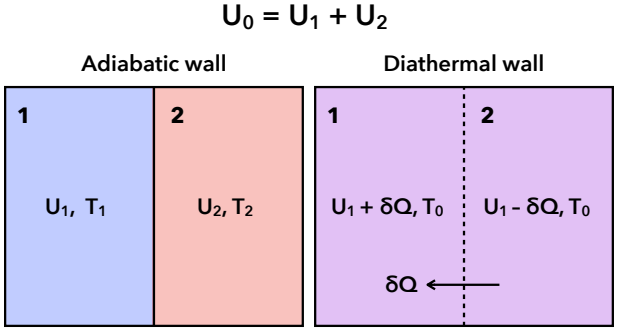

Figure 3: Two subsystems contained in adiabatic enclosures with different temperatures T_1 and T_2 with $T_1 < T_2$ will experience a spontaneous heat transfer when the adiabatic wall is replaced with a diathermal wall.

into two sub-systems via an adiabatic wall, and we notice initially that they have two different temperatures T_1 and T_2, where $T_1 < T_2$. We thus have a "hot" region and a "cold" region inside of our isolated system. The total energy of the isolated composite system is simply the sum of the energy of the two sub-systems, $U_0 = U_1 + U_2$. If we now replace the adiabatic wall with a diathermal wall, an amount of heat $\delta\mathcal{Q}$ will flow between the two sub-systems due to the initial temperature gradient. The effect of this heat transfer is that the energy of sub-system 1 has increased by $\delta\mathcal{Q}$ and the energy of sub-system 2 has decreased by $\delta\mathcal{Q}$. The heat transfer stops only when the temperature of the composite system is uniform everywhere at a value of T_0, which we speculate to lie somewhere in the interval $[T_1, T_2]$. After this process is complete, the total energy of the composite system is unchanged $U_0 = (U_1 + \delta\mathcal{Q}) + (U_2 - \delta\mathcal{Q}) = U_1 + U_2$. However, if we consider the change in entropy of the system due to this spontaneous process $\Delta S = \delta\mathcal{Q}/T_1 - \delta\mathcal{Q}/T_2$, we find that the overall entropy of the system has increased since $T_1 < T_2$. The heat transfer stops only when $T_1 = T_2 = T_0$ since the driving force for heat transfer (*i.e*, the temperature gradient) vanishes; in other words, once the system is at equilibrium, any additional heat transfer would fail to increase the entropy any further since $\Delta S = \delta\mathcal{Q}/T_0 - \delta\mathcal{Q}/T_0 = 0$ J/K.[2] This leads us to the *second law of thermodynamics*, which states that for

[2]Here we consider the thermal energy to be in units of Joules (1 J = 1 N·m = 1 kg·m^2·s^{-2}) and temperature to be in units of Kelvin (K).

an isolated system, the total entropy of the system can never decrease; the total entropy can only increase or remain constant. Using the definition of the second law, we can write the combined first and second law of thermodynamics as

$$dU = TdS - PdV + \sum_i \mu_i dN_i + \Phi dQ, \tag{4}$$

which indicates that the internal energy of a system is a function of a set of *natural variables* $U = U(S, V, N_i, Q)$. This particular set of variables are said to be *extensive variables*, since their values scale proportionally with system size, while their conjugate variables T, P, μ, and Φ are said to be *intensive variables* that are independent of system size and have the additional property that they are equal everywhere within a system at equilibrium. Furthermore, Eq. 4 is said to be a *fundamental relation* that one can use to completely define the state of a thermodynamic system. The caveat to this is that it is also necessary to identify the *equations of state*[3] that relate the intensive variables to the extensive variables in the system

$$\begin{aligned} T = T(S, V, N_i, Q) &= \left(\frac{\partial U}{\partial S}\right)_{V,N_i,Q} \\ P = P(S, V, N_i, Q) &= -\left(\frac{\partial U}{\partial V}\right)_{S,N_i,Q} \\ \mu_i = \mu_i(S, V, N_i, Q) &= \left(\frac{\partial U}{\partial N}\right)_{S,V,N_j\neq N_i,Q} \\ \Phi = \Phi(S, V, N_i, Q) &= \left(\frac{\partial U}{\partial Q}\right)_{S,V,N_i} \end{aligned} \tag{5}$$

Thus, given a fundamental relation of a system and its associated equations of state, one can fully understand a thermodynamic system.

2.2 Alternative forms of the fundamental relation

While Eq. 4 is an important result embodying the first two laws of thermodynamics, it is not always the most convenient form of the fundamental relation to use when discussing chemical or electrochemical thermodynamics. This stems primarily from the fact that the internal energy depends on extensive quantities such as entropy, volume, particle number, and charge, which are infeasible to rigorously control in laboratory settings. Instead, it is more useful to consider forms of the fundamental relation that depend on temperature, pressure, chemical potential, or voltage since these quantities can be more readily manipulated in experiments. These alternative forms can be derived using a mathematical technique called *Legendre transformation*, which provides an alternative but equivalent representation of a function $f(x)$ in terms of its derivative $m(x) = f'(x)$ and its associated tangent line's y-intercept b

$$b(m) = f(x) - m(x)x. \tag{6}$$

In Fig. 4, we demonstrate the procedure for a one-dimensional parabolic function.[12] For higher-dimensional cases, such as the thermodynamic potentials we are considering here, one can perform an analogous procedure using partial derivatives. Because the intensive variables we aim to replace the extensive variables with are defined as partial derivatives of the internal energy (Eq. 5), we are able to employ this technique to derive a variety of fundamental relations. To demonstrate this, we must first consider the internal energy in its Euler form[4]

$$U = TS - PV + \sum_i \mu_i N_i + \Phi Q. \tag{7}$$

[3]Here we see that the intensive variables can be equivalently expressed as partial derivatives of the internal energy with respect to their extensive conjugate variables. This follows from the fact that the internal energy is a state function so we consider an infinitesimal change in internal energy to be an exact differential:

$$dU = \left(\frac{\partial U}{\partial S}\right)_{V,N_i,Q} dS + \left(\frac{\partial U}{\partial V}\right)_{S,N_i,Q} dV + \sum_i \left(\frac{\partial U}{\partial N}\right)_{S,V,N_j\neq N_i,Q} dN_i + \left(\frac{\partial U}{\partial Q}\right)_{S,V,N_i} dQ.$$

[4]Extensive quantities such as the internal energy are said to be first order homogenous functions, which obey the property $f(\lambda x_1, \lambda x_2, \ldots, \lambda x_n) = \lambda f(x_1, x_2, \ldots, x_n)$, where λ is an arbitrary constant. If we compute the derivative of both sides with

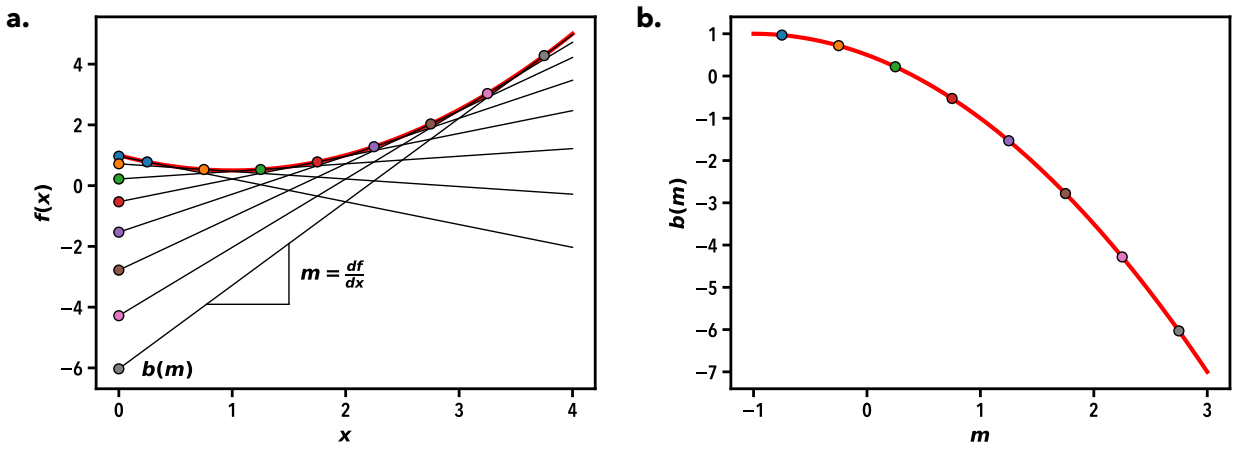

Figure 4: The procedure for computing the Legendre transform of a function $f(x)$ involves (a) obtaining the set of tangent line slopes $m = df/dx$ of the underlying function $f(x)$ and their associated set of y-intercepts $b = b(m)$ for the entire domain of $f(x)$. The original function $f(x)$ is transformed (b) to $b(m)$, which can be viewed as an alternative yet equivalent representation of the underlying function $f(x)$.

As an example, if we wish to obtain a fundamental relation with the set of natural variables (S, P, N_i, Q), we may compute the Legendre transform of the internal energy with respect to the volume

$$H = U - \left(\frac{\partial U}{\partial V}\right) V = U + PV, \tag{8}$$

where the new thermodynamic potential H introduced above is known as the *enthalpy* of a system. Using Eq. 4, we can obtain the desired fundamental relation by computing the differential of Eq. 8

$$dH = dU + PdV + VdP = TdS + VdP + \sum_i \mu_i dN_i + \Phi dQ. \tag{9}$$

We can perform single Lengendre transforms as we have done above, or we can perform multiple Legendre transforms to obtain a fundamental relation that has more than one intensive variable in its set of natural variables. For example, the Gibbs free energy G has the set of natural variables (T, P, N_i, Q), and its fundamental relation can be obtained via the double Legendre transform

$$G = U - TS + pV \quad \longrightarrow \quad dG = -SdT + VdP + \sum_i \mu_i dN_i + \Phi dQ. \tag{10}$$

Using this approach, a variety of fundamental relations can be derived from the combined first and second law, several of which have been summarized below in Table 1.

3 Statistical mechanics

Up until this point, we have mainly considered the thermodynamics of macroscopic systems and introduced several useful fundamental relations. While these equations enable us to at least in principle identify equilibrium states, they do not provide any information about the microscopic details that are needed to effectively understand the properties of functional materials. Such a detailed view can be obtained by considering

respect to λ, we obtain $\sum_i \left(\frac{\partial f}{\partial \lambda x_i}\right) x_i = f(x_1, x_2, \ldots, x_n)$. Because λ is just a constant, we can consider the case of $\lambda = 1$, which yields $\sum_i \left(\frac{\partial f}{\partial x_i}\right) x_i = f(x_1, x_2, \ldots, x_n)$. The latter is referred to as an Euler relation as it obeys Euler's theorem for homogenous functions.[12]

Table 1: Summary of important thermodynamic potentials, their Legendre transforms, and their associated fundamental relations.

Thermodynamic potential	**Legendre transform**	**Fundamental relation**
Enthalpy	$H = U + PV$	$dH = TdS + VdP + \sum_i \mu_i dN_i + \Phi dQ$
Helmholtz free energy	$A = U - TS$	$dA = -SdT - PdV + \sum_i \mu_i dN_i + \Phi dQ$
Gibbs free energy	$G = U - TS + PV$	$dG = -SdT + VdP + \sum_i \mu_i dN_i + \Phi dQ$
Electrochemical enthalpy	$F = U - \Phi Q$	$dF = TdS - PdV + \sum_i \mu_i dN_i - Qd\Phi$
Electrochemical free energy	$\mathscr{F} = U - TS - \Phi Q$	$d\mathscr{F} = -SdT - PdV + \sum_i \mu_i dN_i - Qd\Phi$
Grand potential	$\phi = U - TS - \mu_j N_j$	$d\phi = -SdT - PdV - N_j d\mu_j + \sum_{i\neq j} \mu_i dN_i + \Phi dQ$
Electrochemical grand potential	$\varphi = U - TS - \mu_j N_j - \Phi Q$	$d\varphi = -SdT - PdV - N_j d\mu_j + \sum_{i\neq j} \mu_i dN_i - Qd\Phi$

the *statistical mechanics* of a system, which provides a link between the configuration and motion of a set of particles and the observed macroscopic properties of a thermodynamic system. In what follows, a brief overview of the statistical mechanics of electrochemical interfaces will be provided.

3.1 Preliminaries

In statistical mechanics, we consider a system to exist in a certain *macrostate*, which is a particular thermodynamic state specified by a set of fixed properties such as constant particle number N, constant volume V, and constant temperature T. Each macrostate is associated with a vast set or *ensemble* of *microstates*, where a microstate can be viewed as a copy of the system whose constituent particles adopt different configurations and momenta. The set of microstates corresponding to a given macrostate spans all of the possible configurations and momenta that conform to the particular macrostate. We can furthermore associate each microstate with a set of $6N$ coordinates $\{\boldsymbol{r}^N, \boldsymbol{p}^N\}$ describing the positions $\boldsymbol{r}$ and the momenta $\boldsymbol{p}$ of the N particles in the system, as well as an energy $E = \mathcal{H}(\boldsymbol{r}^N, \boldsymbol{p}^N)$ that is determined by a suitable *Hamiltonian* $\mathcal{H} = \mathcal{T} + \mathcal{V}$ that accounts for the kinetic energy $\mathcal{T}(\boldsymbol{p}^N) = \sum_i^N |\boldsymbol{p}_i|^2/2m_i$ and the potential energy $\mathcal{V}(\boldsymbol{r}^N)$ of the particles. Individual microstates can additionally be viewed as points in a $6N$-dimensional space that is referred to as the *phase space* of the system. We can therefore quantify the "size" of a macrostate by the volume it occupies in phase space, or equivalently the number of microstates it contains. Thus within any given macrostate, there are an enormous number of possible microstates that the system could be in at any given time; however, as we will discuss shortly, certain microstates may be more probable than others. It follows then, that the subset of microstates with the highest probabilities can be identified to be the equilibrium states of a system.

The probability of the system being in a particular microstate is determined by the Boltzmann distribution, which for the example (N, V, T) ensemble discussed above, would be expressed as

$$P(\boldsymbol{r}^N, \boldsymbol{p}^N) = \frac{\exp\left[-\beta\mathcal{H}(\boldsymbol{r}^N, \boldsymbol{p}^N)\right]}{\frac{1}{h^{3N}N!}\int_\Omega d\boldsymbol{p}^N d\boldsymbol{r}^N \exp\left[-\beta\mathcal{H}(\boldsymbol{r}^N, \boldsymbol{p}^N)\right]} = \frac{\exp\left[-\beta\mathcal{H}(\boldsymbol{r}^N, \boldsymbol{p}^N)\right]}{\mathscr{Q}}, \tag{11}$$

where $\mathscr{Q}$ is the partition function of the system that involves $6N$ integrals over the region of phase space Ω occupied by the macrostate, and $\beta = 1/k_B T$ is known as the thermodynamic beta, where k_B is the

Boltzmann constant. Because each volume element of phase space $d\boldsymbol{p}d\boldsymbol{r}$ has dimensions of action, it is common by convention to introduce a factor of h^{-3} for each element to obtain a dimensionless probability, where h is Planck's constant. Furthermore, in the case that we consider particles to be indistinguishable from one another, a permutation factor $(N!)^{-1}$ is introduced to account for the identical configurations that arise from interchanging the positions of indistinguishable particles. Macroscopic properties of the system such as the internal energy, volume, and charge can be computed as an expectation value or an *ensemble average* of the system. For example, the ensemble average of an arbitrary property A of a classically interacting system is computed by integrating a weighted probability distribution over the region of phase space occupied by the macrostate

$$\langle A \rangle = \frac{1}{h^{3N} N!} \int_{\Omega} d\boldsymbol{p}^N d\boldsymbol{r}^N A(\boldsymbol{r}^N, \boldsymbol{p}^N) P(\boldsymbol{r}^N, \boldsymbol{p}^N) \tag{12}$$

where here we see that the pre-factor $(h^{3N} N!)^{-1}$ cancels when the expectation value is computed. In practice, this expression can be simplified by analytically solving the momentum integrals over the phase space of the system.[5] This enables us to focus solely on the contribution of the configuration-dependent potential energy $E_i = \mathcal{V}(\boldsymbol{r}_i^N)$ when computing expectation values, which means that the probability distribution that must be considered depends only on the configurational space of the system and is thus proportional to the overall probability $\mathcal{P}(\boldsymbol{r}^N) \propto P(\boldsymbol{r}^N, \boldsymbol{p}^N)$. Similarly, we also consider a configuration-dependent partition function $Z \propto \mathscr{Q}$. And finally, the integrals over the configurational space of the system may be replaced by a summation over the individual microstates that are accessible within the given macrostate. This allows us to rewrite the probability distribution as

$$\mathcal{P}_i = \frac{\exp\left[-\beta E_i\right]}{\sum_j \exp\left[-\beta E_j\right]} = \frac{1}{Z} \exp\left[-\beta E_i\right]. \tag{13}$$

Accordingly, ensemble averages are analogously obtained by computing a weighted sum over the phase space of the system

$$\langle A \rangle = \sum_i A_i \mathcal{P}_i. \tag{14}$$

3.2 The electrochemical canonical (N, V, T, Φ) ensemble

In the electrochemical canonical ensemble, we consider a closed system to be in contact with a large reservoir that is held at a fixed temperature T and a fixed electrode potential Φ.[14] The system is able to freely exchange heat and electrons with the reservoir, and at equilibrium, the energy and the charge of the system will fluctuate around their equilibrium values. Furthermore, as in classical thermodynamics, the temperature and the electrode potential of the system will be equal to that of the reservoir at equilibrium. It can additionally be shown[6] that the Boltzmann distribution for the (N, V, T, Φ) ensemble can be expressed as

$$\mathcal{P}_i = \frac{1}{Z} \exp\left[-\beta(E_i - \Phi Q_i)\right]. \tag{15}$$

The validity of this definition for the Boltzmann distribution can be demonstrated by calculating the entropy of the system via the Gibbs entropy formula

$$S = -k_B \sum_i \mathcal{P}_i \ln \mathcal{P}_i. \tag{16}$$

Inserting Eq. 15 into Eq. 16, we obtain

$$S = \frac{\langle E \rangle}{T} - \frac{\Phi \langle Q \rangle}{T} + k_B \ln Z, \tag{17}$$

[5] For a single component system, it can be shown that the momentum integrals $I = \int_{-\infty}^{\infty} d\boldsymbol{p}^N \exp\left[-\beta \sum_i |\boldsymbol{p}_i|^2 / 2m\right]$ evaluate to $I = (\sqrt{2m\pi k_B T})^{3N}$. This allows the partition function to be expressed as $\mathscr{Q} = (\Lambda^{3N} N!)^{-1} \int d\boldsymbol{r}^N \exp[-\beta \mathcal{V}(\boldsymbol{r}^N)] = Z/\Lambda^{3N} N!$. Here $\Lambda = \sqrt{h^2/2\pi m k_B T}$ is the thermal de Broglie wavelength, and Z is referred to as the configurational integral. It is straightforward to show that this result may be generalized to treat classically interacting multi-component systems.

[6] The Boltzmann distribution can be obtained in a straightforward manner using Lagrange multipliers to maximize the Gibbs entropy of the system, subject to the constraints that the probability remains normalized $\sum_i \mathcal{P}_i = 1$ and that the probability distribution recovers the expectation values of the energy $\langle E \rangle = \sum_i \mathcal{P}_i E_i$ and charge $\langle Q \rangle = \sum_i \mathcal{P}_i Q_i$.

where we have made use of Eq. 14. After some minor algebra, we find

$$-k_B T \ln Z = \langle E \rangle - TS - \Phi \langle Q \rangle. \tag{18}$$

Comparing this equation to the Euler relation for the electrochemical free energy, $\mathscr{F} = U - TS - \Phi Q$, we can readily identify $\mathscr{F} = -k_B T \ln Z$, $U = \langle E \rangle$ and $Q = \langle Q \rangle$. Thus, the electrochemical free energy $\mathscr{F}$ and the entropy S depend explicitly on the partition function Z, while the internal energy and the charge of the system are obtained as expectation values of fluctuating quantities. It also straightforward to show that the average charge and the internal energy can be expressed in terms of logarithmic derivatives of the partition function

$$\langle Q \rangle = \sum_i Q_i \mathcal{P}_i = \frac{1}{\beta} \frac{\partial \ln Z}{\partial \Phi} = -\left(\frac{\partial \mathscr{F}}{\partial \Phi} \right)_{N,V,T} \tag{19}$$

$$\langle E \rangle = \sum_i E_i \mathcal{P}_i = \Phi \langle Q \rangle - \frac{\partial \ln Z}{\partial \beta}. \tag{20}$$

At equilibrium, heat and charge fluctuate randomly between the system and the reservoir, indicating that the fluctuations $\Delta E = E_i - \langle E \rangle$ and $\Delta Q = Q_i - \langle Q \rangle$ may also be considered to be random variables. For a general fluctuation $\Delta A = A_i - \langle A \rangle$, it can be shown that the mean of the fluctuation vanishes $\langle \Delta A \rangle = 0$, verifying that the energy and the charge distributions are centered on their means. The spread of the distributions can be quantified as the mean square of the fluctuations $\langle (\Delta A)^2 \rangle = \langle A_i^2 - 2A_i \langle A \rangle + \langle A \rangle^2 \rangle = \langle A^2 \rangle - \langle A \rangle^2$, which is nothing other than the *variance* of the distribution of fluctuations. It can be shown that the variance of a fluctuation is related to the second order logarithmic derivative of the partition function with respect to the intensive conjugate variable of the fluctuating quantity. For example, when considering the fluctuation of the charge in the system, we observe the following relation to hold

$$\frac{\partial \langle Q \rangle}{\partial \Phi} = \frac{1}{\beta} \frac{\partial^2 \ln Z}{\partial \Phi^2} = \frac{1}{\beta} \frac{\partial}{\partial \Phi} \left[\frac{1}{Z} \frac{\partial Z}{\partial \Phi} \right] = \frac{1}{\beta} \left[\frac{1}{Z} \frac{\partial^2 Z}{\partial \Phi^2} - \frac{1}{Z^2} \left(\frac{\partial Z}{\partial \Phi} \right)^2 \right] = \beta \left[\langle Q^2 \rangle - \langle Q \rangle^2 \right]. \tag{21}$$

The latter is quite interesting as it provides a connection between the macroscopic charge-voltage response of an electrochemical interface and the fluctuating charge on the electrode. In fact, this is the definition of the differential capacitance of the electrode-solution interface, which allows us to write

$$C_0 = \frac{d\sigma}{d\Phi} = \frac{1}{A} \frac{d\langle Q \rangle}{d\Phi} = \frac{\beta}{A} \left[\langle Q^2 \rangle - \langle Q \rangle^2 \right], \tag{22}$$

where $\sigma = Q/A$ is the surface charge density on the electrode, and C_0 is the *areal differential capacitance*. The exactness of this definition is guaranteed in the thermodynamic limit where the total number of particles $N_{\text{tot}} = \sum_i N_i$ in the system approaches Avogadro's number. To show this, we consider the fact that the charge and the capacitance of a system are extensive quantities and can be expressed in terms of a scalar λ as $\langle Q \rangle = \lambda \langle Q \rangle_{\text{ref}}$ and $AC_0 = \lambda A_{\text{ref}} C_0$. Here, we define λ in terms of a reference system that has a fixed stoichiometry and a total number of particles $N_{\text{ref}} = \sum_i N_i^{\text{ref}}$, so that the total number of particles in the scaled system are $N_{\text{tot}} = \sum_i N_i = \lambda N_{\text{ref}}$. Next, we define the amplitude of the charge fluctuation to be the root mean square fluctuation $\Delta Q_{\text{rms}} = (\langle Q^2 \rangle - \langle Q \rangle^2)^{1/2}$, which is nothing other than the standard deviation of the charge fluctuations. If we now consider the ratio of the fluctuation amplitude to the average charge in the system

$$\frac{\Delta Q_{\text{rms}}}{\langle Q \rangle} = \sqrt{\frac{AC_0}{\beta \langle Q \rangle^2}} = \sqrt{\frac{\lambda A_{\text{ref}} C_0}{\beta \lambda^2 \langle Q \rangle_{\text{ref}}^2}} = \sqrt{\frac{A_{\text{ref}} C_0}{\beta \langle Q \rangle_{\text{ref}}^2}} \frac{1}{\sqrt{\lambda}}, \tag{23}$$

we find that the charge fluctuations become vanishingly small in comparison to the average charge of the system in the thermodynamic limit where $\lambda \to \infty$. As a consequence of this, the charge distributions become very sharply peaked about their means.

The differential capacitance is one example of what is known as a *response function* or a *susceptibility* in statistical mechanics. Several other response functions can be defined in the (N, V, T, Φ) ensemble that consist of the response of an extensive quantity to variations in either their conjugate intensive variable or

to another intensive variable that is controlled by the reservoir. It can be shown that given two sets of conjugate variables (X, F_X) and (Y, F_Y), the following relation generally holds

$$\langle \Delta X \Delta Y \rangle = \langle XY \rangle - \langle X \rangle \langle Y \rangle = \frac{1}{\beta} \frac{\partial \langle X \rangle}{\partial F_Y} = \frac{1}{\beta} \frac{\partial \langle Y \rangle}{\partial F_X}, \tag{24}$$

which states that the *covariance* of fluctuations in X and Y are related to the response of $\langle X \rangle$ to variations in the externally controlled potential F_Y and *vice versa*. A number of response functions can be derived for the (N, V, T, Φ) ensemble, several of which have been summarized below in Table 2.

Table 2: Summary of several useful response functions in the electrochemical canonical (N, V, T, Φ) ensemble.

Response function	
Internal energy - Voltage	$\frac{\partial \langle E \rangle}{\partial \Phi} = \beta[\langle EQ \rangle - \langle E \rangle \langle Q \rangle]$
Differential capacitance, AC_0	$\frac{\partial \langle Q \rangle}{\partial \Phi} = \beta[\langle Q^2 \rangle - \langle Q \rangle^2]$
Constant volume heat capacity, C_V	$\frac{\partial \langle E \rangle}{\partial T} = k_B \beta^2 \left[\langle E^2 \rangle - \langle E \rangle^2 - \frac{\Phi}{\beta} \frac{\partial \langle E \rangle}{\partial \Phi} \right]$
Charge - Temperature	$\frac{\partial \langle Q \rangle}{\partial T} = k_B \beta^2 \left[\frac{1}{\beta} \frac{\partial \langle E \rangle}{\partial \Phi} - \frac{\Phi}{\beta} \frac{\partial \langle Q \rangle}{\partial \Phi} \right]$

3.3 The electrochemical grand canonical (μ, V, T, Φ) ensemble

In the electrochemical grand canonical ensemble, we consider an open system that is in contact with a large reservoir that is held at a fixed temperature T, a fixed electrode potential Φ, and a fixed chemical potential μ_j for a species j.[15] The system is able to exchange heat, electrons, and j particles with the reservoir, and at equilibrium, the energy, charge, and particle number of the system will fluctuate around their equilibrium values. The Boltzmann distribution in the (μ, V, T, Φ) ensemble can be expressed as

$$\mathcal{P}_k = \frac{1}{\mathcal{Z}} \exp\left[-\beta(E_k - \mu_j (N_j)_k - \Phi Q_k)\right] = \frac{1}{\mathcal{Z}} \exp\left[-\beta(F_k - \mu_j (N_j)_k)\right], \tag{25}$$

where we show explicitly that the Boltzmann factor can be rewritten in terms of the electrochemical enthalpy $F_k = E_k - \Phi Q_k$. Following the same procedure we employed in the previous section, we compute the Gibbs entropy of the system as

$$S = \frac{\langle E \rangle}{T} - \frac{\mu_j \langle N_j \rangle}{T} - \frac{\Phi \langle Q \rangle}{T} + k_B \ln Z, \tag{26}$$

which upon rearrangement leads to the definition of the electrochemical grand potential

$$\varphi = -k_B T \ln \mathcal{Z} = \langle E \rangle - TS - \mu_j \langle N_j \rangle - \Phi \langle Q \rangle. \tag{27}$$

Similar to the energy and charge in the (N, V, T, Φ) ensemble, the mean particle number can be expressed in terms of a logarithmic derivative of the partition function

$$\langle N_j \rangle = \frac{1}{\beta} \frac{\partial \ln \mathcal{Z}}{\partial \mu_j} = -\left(\frac{\partial \varphi}{\partial \mu_j} \right)_{T, V, \Phi, \mu_k \neq \mu_j}. \tag{28}$$

Finally, a number of response functions can be defined in the (μ, V, T, Φ) ensemble that describe the response of unconstrained extensive quantities to variations in the electrode potential, chemical potential, and temperature. Several of these response functions are summarized below in Table 3.

Table 3: Summary of several useful response functions in the electrochemical grand canonical (μ, V, T, Φ) ensemble. The response functions listed in Table 2 (excluding the (N, V, T, Φ) heat capacity) also exist in the (μ, V, T, Φ) ensemble, but are omitted for brevity.

Response function	
Particle number - Voltage	$\frac{\partial \langle N_j \rangle}{\partial \Phi} = \beta[\langle N_j Q \rangle - \langle N_j \rangle \langle Q \rangle]$
Internal energy - Chemical potential	$\frac{\partial \langle E \rangle}{\partial \mu_j} = \beta[\langle E N_j \rangle - \langle E \rangle \langle N_j \rangle]$
Particle number - Chemical potential	$\frac{\partial \langle N_j \rangle}{\partial \mu_j} = \beta[\langle N_j^2 \rangle - \langle N_j \rangle^2]$
Charge - Chemical potential	$\frac{\partial \langle Q \rangle}{\partial \mu_j} = \beta[\langle Q N_j \rangle - \langle Q \rangle \langle N_j \rangle]$
Constant volume heat capacity, C_V	$\frac{\partial \langle E \rangle}{\partial T} = k_B \beta^2 \left[\langle E^2 \rangle - \langle E \rangle^2 - \frac{\mu_j}{\beta} \frac{\partial \langle E \rangle}{\partial \mu_j} - \frac{\Phi}{\beta} \frac{\partial \langle E \rangle}{\partial \Phi} \right]$
Particle number - Temperature	$\frac{\partial \langle N_j \rangle}{\partial T} = k_B \beta^2 \left[\frac{1}{\beta} \frac{\partial \langle E \rangle}{\partial \mu_j} - \frac{\mu_j}{\beta} \frac{\partial \langle N_j \rangle}{\partial \mu_j} - \frac{\Phi}{\beta} \frac{\partial \langle N_j \rangle}{\partial \Phi} \right]$
Charge - Temperature	$\frac{\partial \langle Q \rangle}{\partial T} = k_B \beta^2 \left[\frac{1}{\beta} \frac{\partial \langle E \rangle}{\partial \Phi} - \frac{\mu_j}{\beta} \frac{\partial \langle N_j \rangle}{\partial \Phi} - \frac{\Phi}{\beta} \frac{\partial \langle Q \rangle}{\partial \Phi} \right]$

3.4 Computational methods

Leading up to this point, we have recapitulated thermodynamics and statistical mechanics, and we have additionally demonstrated how the effects of an applied electrode potential may be included within the developed theoretical framework. We note that while statistical mechanics provides a formally exact answer for how a collection of particles behaves under a set of externally applied potentials, it stops short of providing an approach for performing practical calculations to obtain useful numerical results. Such approaches are necessary to guide the design and understanding of physical material systems. That being said, a significant effort has been made since the inception of statistical mechanics to develop the computational tools and methods needed to obtain reliable estimates of material properties from atomistic models. In general, two major obstacles must be overcome in order to achieve satisfactory results. The first challenge to address is how to define the many-body potential $\mathcal{V}(\boldsymbol{r}^N)$ that describes the interactions between the particles in the system. In condensed matter systems such as the electrode-electrolyte interfaces we consider herein, quantum effects generally become important and computationally demanding quantum mechanical calculations must be performed to explicitly treat the electrons in the system. As will be discussed in the next section, modern approaches rely on *density functional theory* (DFT) calculations, which offer a balance between computational efficiency and accuracy for the ground state properties of most material systems. The second challenge to be addressed is that the thermodynamic averages we aim to compute require integrals to be carried out over the $6N$-dimensional phase space of the system. Because of this, attempts to directly compute the partition function in the thermodynamic limit where statistical mechanics becomes precise requires the solution of an astronomically large number of integrals on the order of 10^{23}. We therefore regard the partition function to be an essentially unknowable quantity, and as will be discussed shortly, several methods have been developed to circumvent the need for its direct evaluation.[7]

One popular approach to obtaining the equilibrium properties of an atomistic system is to perform a *molecular dynamics* simulation, which evolves a collection of atoms through space and time by integrating

[7]There are, however, some exceptional cases where the partition function can be written as a closed-form expression, such as the 1D and 2D Ising models that describe the magnetization of a lattice of binary spins. The latter are often regarded to be "toy models" in view of their simplicity.

Newton's equations of motion

$$\boldsymbol{F}_i(t) = m_i \boldsymbol{a}_i(t) = -\nabla_{\boldsymbol{r}_i} \mathcal{V}(\boldsymbol{r}^N, t) \tag{29}$$

$$\boldsymbol{v}_i(t) = \int_{t_0}^{t} \boldsymbol{a}_i(s) ds + \boldsymbol{v}_i(t_0) \tag{30}$$

$$\boldsymbol{r}_i(t) = \int_{t_0}^{t} \boldsymbol{v}_i(s) ds + \boldsymbol{r}_i(t_0), \tag{31}$$

where $\boldsymbol{F}_i(t)$, $\boldsymbol{a}_i(t)$, $\boldsymbol{v}_i(t)$, and $\boldsymbol{r}_i(t)$ are the time-dependent force, acceleration, velocity, and position of atom i, respectively. Ensemble averages are then approximated as a time average across the trajectory that the system takes through phase space after the system has been adequately equilibrated.[8] The time-dependent potential energy of the system $\mathcal{V}(\boldsymbol{r}^N, t)$ that appears in Eq. 29 may be defined *ab initio* using DFT as we have discussed above, or may be approximated using a suitably parametrized model *force field*. Because of their analytic form, the use of force fields considerably extends the length and time scales that may be considered in a molecular dynamics simulation, thereby enabling the simulation of a broader range of phenomena. However, the use of force fields becomes challenging when modeling electrochemical interfaces since the electronic degrees of freedom in the system must be accounted for to accurately model the effects of an applied electrode potential. A number of efforts have been made recently to effectively describe the behavior of electrons within classical force fields resulting in the development of polarizable force fields, charge optimized many body force fields, and reactive force fields that can capture the effects of instantaneous molecular dipole formation, the variation in atomic oxidation states, as well as the formation and breaking of chemical bonds, respectively.[16, 17, 18] Unfortunately, these approaches tend to be *ad hoc* by design and therefore require extensive parametrization and validation work each time a new material system is considered. However, once parameterized, large simulations may be conducted with an accuracy that approaches that of *ab initio* molecular dynamics at a fraction of the computational cost. Nevertheless, in cases where force fields do not yet exist or are challenging to parametrize, *ab initio* molecular dynamics may still be performed to provide a rigorous description of the atomic and electronic degrees of freedom in the system. Of course, the downside to this gain in accuracy and rigor is a highly demanding calculation that may presently require hundreds of processors operating for weeks or even months at a time in order to obtain sufficiently accurate statistics.

While molecular dynamics simulations provide a perfectly valid basis for modeling materials, certain types of phenomena or properties may be challenging to study due to the limited time and length scale of a simulation. Fortunately, we are not restricted to using purely dynamical simulations to sample the microstates of a thermodynamic system. Alternatively, one may employ a *Monte Carlo* method, which facilitates the efficient computation of ensemble averages via a random sampling of the configurational space of a system. Monte Carlo approaches are deemed to be superior to dynamical simulations when studying infrequent events such as the binding of a substrate to an active site in enzyme catalysis or the penetration of radiation through dense media such as the shielding materials used in nuclear reactors. Similarly, Monte Carlo methods are useful for predicting properties that require a large degree of conformational or configurational sampling such as when determining the most probable structure of a protein based on how its underlying peptide chain may fold in on itself, or the composition and structure of an alloy electrode surface at a given temperature, pressure, or electrode potential. In general, Monte Carlo methods excel in any application that requires the evaluation of large multidimensional integrals such as the integrals frequently encountered in statistical physics.[19] The utility of Monte Carlo methods stems from the fact that the accuracy of an estimator $\bar{A}_N$ for an expected value $\langle A \rangle$ improves systematically as the number of independent random samples N drawn from a probability distribution P approaches infinity as a result of the *law of large numbers*, and similarly that the statistical error $\Delta_{\bar{A}_N} = (\langle \bar{A}_n^2 \rangle - \langle A \rangle^2)^{1/2}$ that describes the standard deviation of the estimator for the expected value decreases as $N^{-1/2}$ as a consequence of the *central limit theorem*. In other words, we can always improve the accuracy and precision of our estimate for an expected value by drawing more random samples so long as the samples are independent and identically distributed. This is at variance with conventional numerical quadrature techniques, which require the integration domain to be discretized

[8] The equivalence of time and ensemble averages is posited by the *ergodic hypothesis*, which states that over a long enough simulation time, the microstates associated with a certain energy become equally likely. Thus, over a long enough trajectory of an equilibrated system, the simulation samples the most probable microstates of a system which constitute a large fraction of the phase space volume, thereby approximating the ensemble average.

into a mesh of uniformly spaced points at which a function is evaluated. The total number of points in this mesh grows exponentially as N^d, where N is the number of points along each dimension, and d is the number of dimensions to be considered. Because the accuracy and precision of quadrature techniques improve with increasingly dense meshes, high dimensional systems become prohibitively expensive to treat due to the exponential growth in computational effort. Compared to analogous Monte Carlo integration schemes, achieving systematic improvements in the accuracy and precision of integral estimates via numerical quadrature methods can be challenging. While a number of Monte Carlo algorithms exist in the literature, we will concern ourselves with just one approach in this work that is known widely as the Metropolis algorithm. We will provide a more detailed discussion of this approach in Section 4.3.

4 The quantum-continuum approach

4.1 Overview

In the previous section, a thermodynamic framework that accounts for the effects of an electrode potential on the state of a thermodynamic system was introduced and discussed at a high level. The connection between the net electronic charge and the microscopic properties of the system was underscored, and notable quantities such as the differential capacitance of an electrode-electrolyte interface were defined in terms of statistical fluctuations of unconstrained extensive quantities. The latter quantity is of particular interest in interfacial electrochemical modeling since it describes the response of the electrode surface charge to variations in the applied electrode potential. Physically, these charge variations may occur as the result of either *faradaic* or *non-faradaic* processes that may be measured experimentally via a suitable electroanalytical technique. In a faradaic process, electronic charge is transferred across the electrode-electrolyte interface to participate in electrochemical reactions, whereas in a non-faradaic process, electronic charge accumulates along the electrode surface and the structure of the electrolyte in the vicinity of the interface adjusts in response to the excess charge on the electrode surface. In the limit where non-faradaic processes prevail, the electrode is referred to as an *ideally polarizable electrode* and the electrode-electrolyte interface behaves as a capacitor where electronic charge stored on the electrode surface is compensated by a build up of ionic charge within the electrolyte near the surface. In the opposite limit where faradaic current dominates, the electrode is referred to as an *ideally non-polarizable electrode* and no capacitive charging along the interface takes place. Generally, real electrodes exhibit properties somewhere in between these two extremes and we can take these to be idealized limits, however in certain cases near ideal polarizability can be observed in certain voltage windows that are referred to as *double layer ranges*. It is evident, however, that in order to understand the charge-voltage response of electrodes, we must first understand the structure and properties of what is referred to as the *electric double layer* (EDL), which is composed of the charged electrode surface and the structured electrolyte near the surface.

As depicted schematically in Fig. 5, the EDL generally consists of a *compact layer* and a *diffuse layer*. Within the compact layer, water and specifically adsorbed ions with broken hydration shells may be present proximal to the surface forming what is referred to as an *inner Helmholtz plane*, and hydrated ions and water may be present above this forming what is referred to as an *outer Helmholtz plane*, or *Stern layer*. The ions present within the compact layer are generally regarded to be immobile and form planes of charge that are situated at a distance that is on the order of the ionic radius or hydrated ionic radius from the surface (or roughly 3-5 Å). Unlike the ions in the compact layer, the ions present in the diffuse layer are fairly mobile and form a space charge region that can extend approximately 10-100 nm into the bulk of the electrolyte.[20] This length scale is problematic for first principles calculations, however, since it would require an immense number of water molecules and ions to be considered introducing an astronomical number of degrees of freedom into the calculation. As will be discussed shortly, it is a common practice to employ a multiscale modeling approach in which only a small portion of the calculation domain is treated quantum mechanically to retain sufficient accuracy, while the remainder of the calculation domain is treated in a simplified manner to greatly improve the speed of the calculation. In the examples that will be discussed below, we will see how an embedded polarizable continuum model can be employed to simplify the treatment of the electrode-electrolyte interface. The latter forms the basis of the *quantum-continuum approach* to first-principles electrochemical modeling.

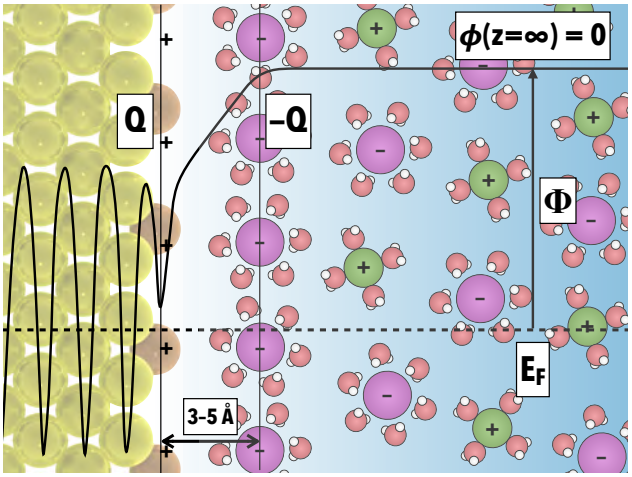

Figure 5: The electric double layer consists of a charged electrode surface and often a combination of a compact layer of ions adjacent to the surface and a diffuse layer of ions that extend into the bulk of the electrolyte. The electric double layer screens the interfacial electric field generated by the charged surface, as depicted by the electrostatic potential of the interface shown as the solid black curve. The converged potential $\phi(z = \infty)$ is aligned to zero by convention in the bulk of the electrolyte to simplify the computation of the voltage to $\Phi = -E_F$, where E_F is the Fermi level of the electrode denoted by the dashed line.

4.2 Electric double layer (EDL) models

To date, several models with varying complexity have been proposed to describe the distribution of ionic charge within an aqueous electrolyte. In order to preface our discussion of the main EDL models and how they describe the charge-voltage response of model electrochemical interfaces, it is necessary to first discuss how the voltage on an electrode is defined in this context. As shown in Fig. 5, the voltage Φ on an electrode is defined as the work required to transfer an electron from the electrode to the bulk of the electrolyte $\Phi = -e_0\phi(z = \infty) - E_F$, where $-e_0$ is the charge of an electron, $\phi(z = \infty)$ is the electrostatic potential of the interfacial system far from the electrode surface in the bulk of the electrolyte, and E_F is the Fermi level (or chemical potential) of the electrons in the electrode. In practice, we align the potential to be zero in the bulk of the electrolyte so that the voltage can be simply computed as $\Phi = -E_F$, where the Fermi level can be readily obtained for a model electrode via quantum-continuum calculations. Here we note that the latter is the definition of the voltage on an absolute scale, and that it is necessary for practical reasons to report this voltage on a relative scale to a well-established reference electrode, such as the standard hydrogen electrode (SHE). This can be achieved by subtracting 4.44 V, which is an estimated value for the absolute SHE potential, or alternatively by aligning the *potential of zero charge* (PZC) of the model electrode to an experimentally measured PZC.[21, 14, 15, 22] Here, the PZC is the voltage at which zero net charge exists on the electrode surface. In general, the PZC of an electrode is sensitive to the composition of the electrolyte it is in contact with. However, if the PZC is observed to have a concentration dependence in a given electrolyte, then specific adsorption effects may be prominent and greater care must be taken in order to properly describe the electrode surface.[20]

The earliest model introduced for the EDL, which is referred to as the *Helmholtz model*, treats the ionic counter charge as a plane of charge sitting a distance λ_H from the electrode surface. The electrode itself is modeled as having an infinite permittivity $\epsilon_M = \infty$, so that the potential within the electrode is a constant ϕ_M. In effect, this model treats the electrode-electrolyte interface as a parallel plate capacitor where the two plates are separated by a dielectric medium. As shown below in Fig. 6, the electrostatic potential varies linearly between the two plates and the interfacial electric field ($E = -d\phi/dz$) is completely screened ($E = 0$) by the ionic countercharge at $z = \lambda_H$, leading to the following piecewise dependence of the

electrostatic potential

$$\phi(z) = \begin{cases} \phi_M = 4\pi\sigma\lambda_H/\epsilon_S & , \quad z < 0 \\ 4\pi\sigma(\lambda_H - z)/\epsilon_S & , \quad 0 \leq z < \lambda_H \\ 0 & , \quad \lambda_H \leq z \end{cases}, \tag{32}$$

where $z = 0$ defines the top of the metal surface, σ is the surface charge density of the metal, and ϵ_S is the permittivity of the solvent layer separating the electronic and ionic charge. The electrode potential is

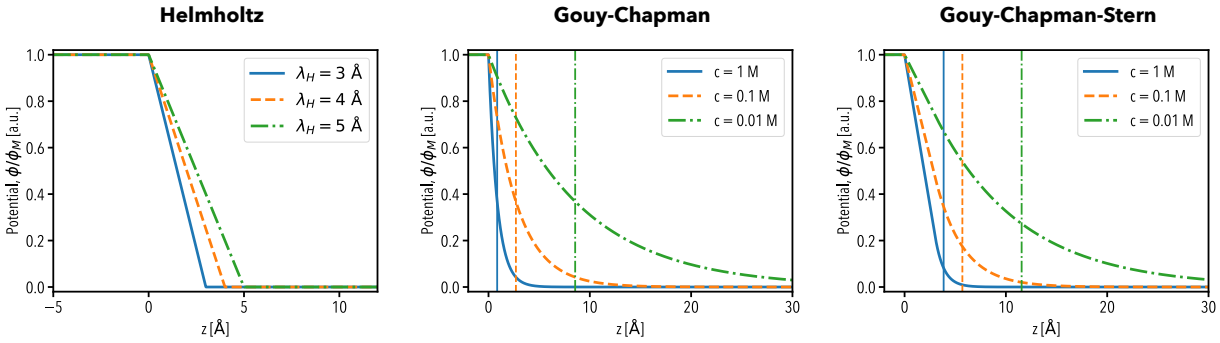

Figure 6: Electrostatic potential profiles for the Helmholtz, Gouy-Chapman, and Gouy-Chapman-Stern models plotted on a relative potential scale. The vertical lines indicate the Debye lengths for 1 M, 0.1 M, and 0.01 M symmetric electrolytes with monovalent ions.

therefore modeled to vary linearly with the surface charge density $\Phi = -4\pi\sigma\lambda_H/\epsilon_S$, and as depicted in Fig. 7, the differential capacitance is a constant parametrized by the Helmholtz layer thickness and the dielectric permittivity

$$C_H = \frac{d\sigma}{d\Phi} = \frac{\epsilon_S}{4\pi\lambda_H}. \tag{33}$$

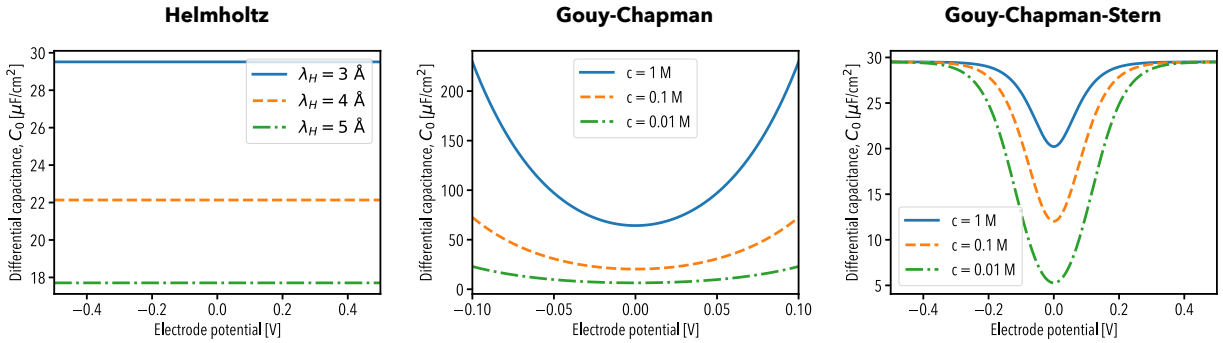

Figure 7: Representative differential capacitance plots for the Helmholtz, Gouy-Chapman, and Gouy-Chapman-Stern models.

Shortly after the introduction of the Helmholtz model, it was quickly realized that it provided an incomplete picture of the EDL as real electrodes exhibit a more complex charge-voltage response that leads to a variable capacitance that passes through a minimum at the PZC of the electrode. The Gouy-Chapman model solves some of these deficiencies by considering the ionic countercharge to be composed of a diffuse layer of ions. In this framework, the ions are assumed to be point particles that are distributed within the electrolyte according to Boltzmann statistics, leading to a diffuse layer charge density

$$\rho_d(z) = z_D c_D \left[\exp\Big(-\beta z_D \phi(z)\Big) - \exp\Big(\beta z_D \phi(z)\Big)\right], \tag{34}$$

where z_D is the valence of the ions (for now we assume symmetric electrolytes with ion charges of $\pm z_D$) and c_d is the concentration of the ions. Here we see that the ionic charge distribution depends upon the interfacial potential, which is generally not known *a priori*. In order to obtain the potential (and therefore the ionic charge distribution), we can insert the Boltzmann distributed density $\rho_D(z)$ into a Poisson equation and solve the resulting *Poisson-Boltzmann equation*

$$\frac{d^2\phi}{dz^2}(z) = -4\pi\frac{\rho_D(z)}{\epsilon_S} = \frac{8\pi z_D c_D}{\epsilon_S}\sinh\Big(\beta z_D\phi(z)\Big). \tag{35}$$

By integrating this equation with the boundary conditions $\phi(z=0)=\phi_M$ and $d\phi/dz \to 0$ as $z\to\infty$, we obtain the derivative of the potential as

$$\frac{d\phi}{dz}(z) = -\left(\frac{32\pi c_D}{\beta\epsilon_S}\right)^{\frac{1}{2}}\sinh\left(\frac{\beta z_D\phi(z)}{2}\right), \tag{36}$$

where we note that the potential and its derivative have opposite signs, indicating that the potential is correctly being screened by the diffuse ionic charge density. By employing Gauss' law ($\oiint \vec{E}\cdot d\vec{S} = 4\pi Q/\epsilon$), we can show that the magnitude of the electric field is proportional to the surface charge density as $d\phi/dz = 4\pi\sigma/\epsilon_S$, allowing us to express the surface charge density at $z=0$ as

$$\sigma = -\left(\frac{2\epsilon_S c_D}{\pi\beta}\right)^{\frac{1}{2}}\sinh\left(\frac{\beta z_D\phi_M}{2}\right). \tag{37}$$

From here, we can obtain the differential capacitance (Fig. 7) of the diffuse ionic countercharge as

$$C_D = \frac{d\sigma}{d\Phi} = C_{D,pzc}\cosh\left(\frac{\beta z_D\Phi}{2}\right), \tag{38}$$

where $C_{D,pzc}$ is the differential capacitance at the PZC of the electrode, and the absolute voltage in this model is taken to be $\Phi = -\phi_M$. The former quantity can be expressed as

$$C_{D,pzc} = \left(\frac{\epsilon_S\beta c_D z_D^2}{2\pi}\right)^{\frac{1}{2}} = \frac{\epsilon_S}{4\pi\lambda_D}, \tag{39}$$

where we have introduced the *Debye length* $\lambda_D = (\epsilon_S/8\pi\beta c_D z_D^2)^{1/2}$, which describes the characteristic screening length of the diffuse counter charge that is sensitive to both the composition and concentration of the bulk electrolyte. Furthermore, by integrating Eq. 36, it can be shown that the potential (Fig. 6) in the system decays exponentially into the electrolyte

$$\phi(z) = \phi_M\exp\left(-\frac{z}{\lambda_D}\right), \tag{40}$$

and that the Debye length is the distance at which the potential has decayed by a factor of $1/e$. Therefore, as the concentration or valence of the ions is increased, the differential capacitance of the interface increases while the Debye length shrinks. Similarly, the capacitance increases at potentials both above and below the PZC as shown in Fig. 7, providing an enhanced qualitative agreement with experimental measurments.

The Gouy-Chapman model is successful to some extent in that it predicts a minimum in the differential capacitance at the PZC, however the model becomes less applicable at modest electrode potentials due to the predicted exponential growth in the capacitance, a feature that is clearly at variance with experimental results. The model also fails in situations where ions become specifically adsorbed to the surface since the point-like ions are free to approach infinitely close to the electrode surface. These issues were rectified by Stern who considered the EDL to contain both Helmholtz and Gouy-Chapman layers. In the Gouy-Chapman-Stern model, the interfacial capacitance is modeled as two capacitors placed in series, leading to the overall capacitance

$$C_S = \left(\frac{1}{C_H}+\frac{1}{C_D}\right)^{-1} = \frac{\epsilon_S}{4\pi}\left(\lambda_H + \frac{\lambda_D}{\cosh(z_d\beta\Phi/2)}\right)^{-1}, \tag{41}$$

where C_H and C_D are the Helmholtz and Gouy-Chapman capacitance, respectively. As shown in Fig. 7, the capacitance exhibits a minimum about the PZC of the electrode and attains a finite value at electrode potentials higher and lower than the PZC in closer agreement with measurements. The electrostatic potential of the Gouy-Chapman-Stern model is depicted in Fig. 6, where we see that the model behaves similarly to the Helmholtz model close to the surface where the potential decays linearly, but then begins to decay exponentially at the interface of the compact and diffuse layers adopting a Gouy-Chapman-like response.

4.3 Example: Silver monolayer stripping on Au(100)

In this section, we demonstrate how the quantum-continuum approach may be applied to model interfacial electrochemical phenomena using planewave density functional theory and a polarizable continuum model.[23] As an example, we consider the electrochemical stability of an atomically thin layer of silver on the gold (100) surface.[15] The calculations that will be described in this section are performed in a periodic cell, and consist of a model gold (100) surface that is composed of seven atomic layers, where the adsorbed silver atoms are included symmetrically on top of the exterior layers of gold. This type of model is commonly referred to as a *symmetric slab*, and we would say that the gold surface is modeled within the *slab-supercell approximation*. The geometry of a typical cell is shown below in Fig. 8, along with the electrostatic potential profile of a silver-covered slab with several different surface charges. In these calculations, the electrode

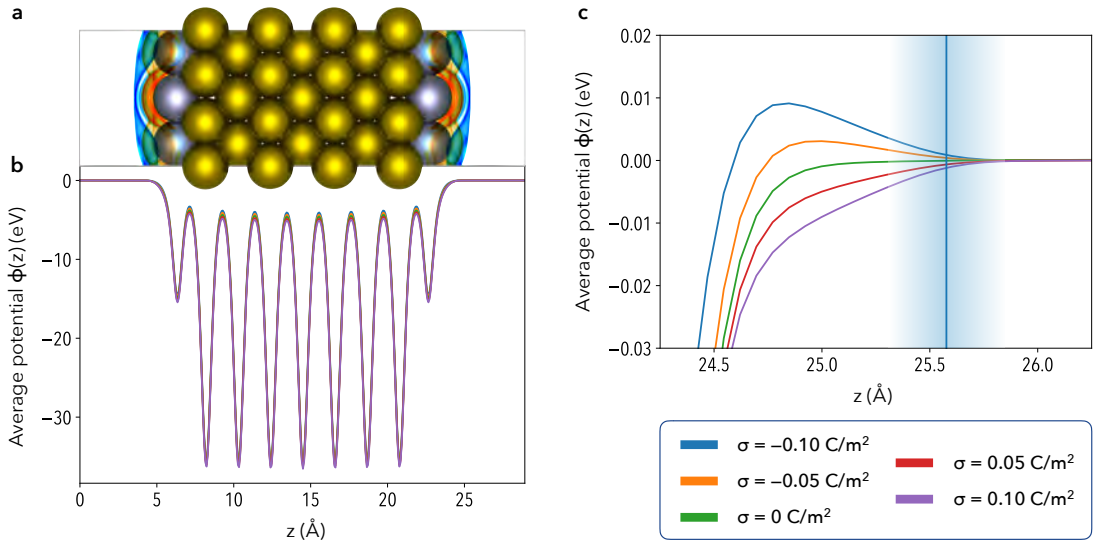

Figure 8: The finite charges placed on the silver-covered gold (100) slab are screened by the planar ionic countercharge in solution. (a) The response of the continuum dielectric at the cavity interface is visualized. Positive/negative polarization charges are shown in red/blue. (b) The electrostatic potential of the electrified slabs are aligned to zero at the edges of the supercell. (c) The Helmholtz layer placed 3 Å from the silver monolayer fully screens the surface charge.

surface is embedded in a polarizable dielectric cavity that enables the description of solvation effects in a computationally efficient manner.[9] Specifically, the mutual interaction of the slab and the continuum dielectric induces the dielectric medium and the electron density to polarize along the interface of the cavity (as shown in Fig. 8a), which mimics the interaction of the metal surface and the dipoles of interfacial water.[23] We additionally consider the electrolyte to be sufficiently concentrated so that the ionic countercharge can

[9]Specifically, these calculations were performed with the planewave DFT code PWscf that is implemented in Quantum ESPRESSO and the *self-consistent continuum solvation model* that is implemented in the Environ module, which serves as a plugin to the PWscf code.[24, 23]

be effectively modeled as a Helmholtz layer. The planar ionic countercharge is positioned 3 Å from the electrode surface and fully screens the surface charge density as shown in Fig. 8c.

The electrochemical stability of silver monolayers on single crystal gold surfaces has been thoroughly studied experimentally. For example, cyclic voltammetry measurements of silver monolayer stripping on the gold (100) surface indicate that the silver monolayer desorbs in three distinct stages, with desorption peaks at 1.25 V, 0.93 V, and 0.72 V versus the SHE in a solution of 5×10^{-3} M Ag_2SO_4 + 0.5 M H_2SO_4 at $T = 298$ K.[25] In order to gain insight into how the presence of surface charge stabilizes the silver monolayer on the surface, we can simulate the adsorption process under different environmental conditions. To begin, we must consider the following electrochemical reaction

$$Ag^+ + e^- + * \rightleftharpoons Ag^*, \tag{42}$$

where $*$ is an available surface site, and Ag^* indicates an adsorbed silver atom on the gold surface. At equilibrium, we have

$$\mu_{Ag^+} - e_0\Phi = \mu_{Ag^*}(\Phi, \theta), \tag{43}$$

where we note that the equilibrium chemical potential of the adsorbed silver atoms $\mu_{Ag^*}(\Phi, \theta)$ has an explicit dependence on the applied electrode potential Φ and silver surface coverage θ. Because the silver atoms may adopt an inordinate number of configurations for a given coverage, it is necessary to sample a number of these configurations to gain a sense of how key thermodynamic properties of the interface may vary. For example, by sampling a series of configurations with neutral surface charge, we may directly probe the variation in the PZC of the electrode as a function of surface coverage, as shown below in Fig. 9a. Here we

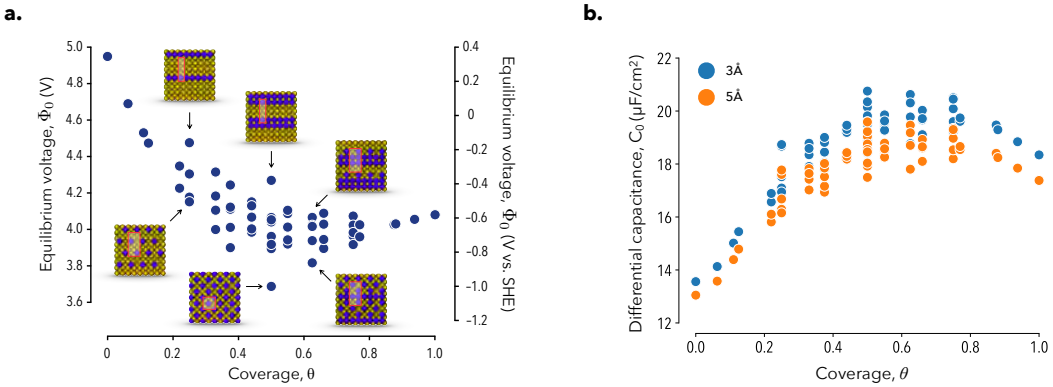

Figure 9: a) Variation in PZCs of silver covered Au(100). b) Variation in the Helmholtz differential capacitance of a variety of silver monolayer configurations on a Au(100) surface.

see the general trend that as the surface coverage increases, the PZC initially begins to shift towards negative potentials, but then begins to increase again after the silver surface coverage exceeds 50%. We also observe that surfaces with compact island-like silver configurations tend to have more positive PZCs as compared to surfaces with dispersed configurations. This indicates that dispersed configurations are accompanied with a larger change in the surface dipole upon monolayer formation as compared to compact configurations. The effect of this is most readily observed in the differential capacitance, which is shown in Fig. 9b for Helmholtz layer thicknesses of 3Å and 5Å. As anticipated, we observe that increasing the Helmholtz layer thickness decreases the capacitance in agreement with Eq. 33. Here we also observe the trend that configurations with lower PZCs tend to have higher capacitance. The origin of this relationship between PZC shift and capacitance enhancement is due to the charge transfer that takes place between the silver adatoms and the gold surface. In general, larger extents of charge transfer occurs for dispersed silver adlayers as compared to condensed adlayers, which is additionally associated with an enhancement in the density of states near the Fermi level of the electrode. The latter enhancement is important as it leads to a concomitant increase in the *quantum capacitance* of the electrode, which is typically on the order of 100-1000 $\mu F/cm^2$ (as compared to 30 $\mu F/cm^2$ for electrolytes) for transition metals. Because the overall capacitance of the interface depends on the

capacitance of the electrode and the capacitance of the electrolyte $C_{tot} = (1/C_Q + 1/C_H)^{-1}$, enhancements in the quantum capacitance increase the overall capacitance of the interface.

Another key thermodynamic property to be assessed is the binding energy of the monolayer per surface site as a function of the silver adlayer coverage. Here we would like to point out that binding energies are enthalpies and not free energies as they do not include entropic contributions, which as we saw previously, requires knowledge of the partition function. Furthermore, understanding how the electrode potential affects binding energies is a prerequisite for determining the equilibrium coverage at a given electrode potential. With this said, we can calculate the binding energy E_B per site of a neutral symmetric slab as

$$E_B = \frac{1}{2N_{\text{sites}}}\left[E(N_{\text{Ag}^*}) - E_{\text{clean}} - N_{\text{Ag}^*}\mu^\circ_{\text{Ag}}\right], \tag{44}$$

where N_{sites} is the total number of sites on one face of the symmetric slab, $E(N_{\text{Ag}^*})$ is the total energy of the neutral silver covered slab with N_{Ag^*} adsorbed silver atoms, E_{clean} is the total energy of the pristine gold (100) slab, and μ°_{Ag} is the chemical potential of silver in its standard reference state as a bulk metal. A charge-dependent binding energy can then be obtained by Taylor expanding the neutral binding energy to second order

$$E_B(Q) = E_B + \left(\frac{\partial E_B}{\partial Q}\right)_{Q=0} Q + \frac{1}{2}\left(\frac{\partial^2 E_B}{\partial Q^2}\right)_{Q=0} Q^2 = E_B + \Phi_0 Q + \frac{Q^2}{2AC_0}, \tag{45}$$

where by definition, the first and second order coefficients are the PZC and the inverse of the differential capacitance. We can subsequently convert the charge-dependent binding energy of each adlayer configuration to an electrochemical enthalpy by the Legendre transform $F = E_B(Q) - \Phi Q$, where $Q = AC_0(\Phi - \Phi_0)$, and the PZC Φ_0 in this expression is configuration-dependent. In principle, the differential capacitance could also be configuration-dependent, however we will just consider the case where it is a constant parameter for all configurations to understand how its value influences the overall thermodynamics of the system. As shown in Fig. 10a, if we set the capacitance to 0 μF/cm^2, which is equivalent to considering each surface with a neutral charge, we find that the binding energies are insensitive to the applied electrode potential. Furthermore, because DFT treats electronic systems at 0 K, only the lowest energy states or *ground states*

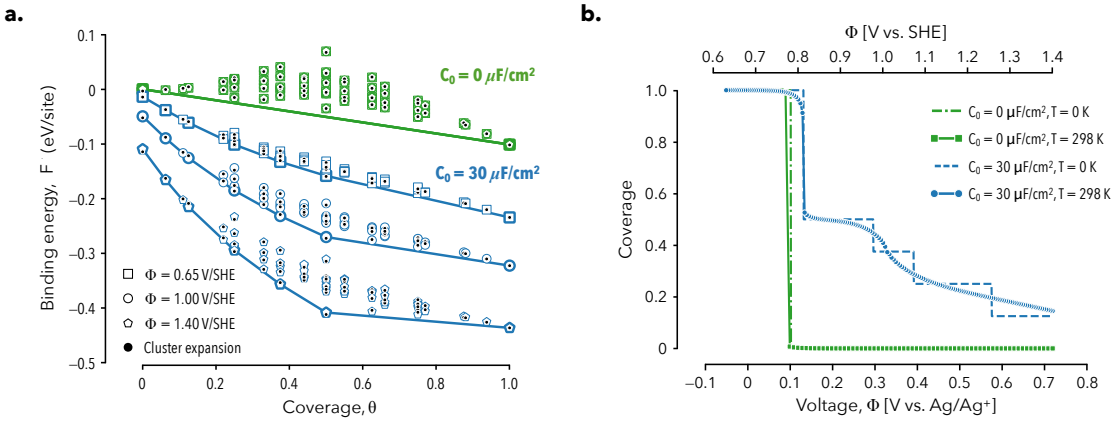

Figure 10: a) Variation in the silver monolayer binding energies on Au(100) as a function of silver coverage and applied electrode potential for $\Phi = 0.65$ V vs. SHE (squares), $\Phi = 1.00$ V vs. SHE (circles), and $\Phi = 1.40$ V vs. SHE (pentagons). b) Silver adsorption isotherms computed for $C_0 = 0$ μF/cm^2 and $C_0 = 30$ μF/cm^2 for $T = 0$ K (dashed lines) and $T = 298$ K (solid lines with markers). The 298 K results were obtained via grand canonical Monte Carlo simulations.

would be available to the surface at this temperature. The lower convex hull or lower envelope formed by these ground states shown as the solid line in the figure indicates that only two stable states exist in this case: the clean gold (100) surface and the same surface with a full silver monolayer. All of the

configurations with intermediate coverages are higher in energy and are therefore inaccessible to the system at 0 K. If we alternatively consider the capacitance to be 30 μF/cm^2, we see distinctly different behavior. In this case, the binding energies become potential-dependent, and we see that several new structures with intermediate coverages migrate to the convex hull, indicating that more configurations with sub-monolayer coverage become stable in the presence of finite surface charge than compared to the neutral case.

In the interest of determining the equilibrium coverage as a function of applied potential, *i.e.*, the *adsorption isotherm* of silver on the gold (100) surface, it is necessary to consider the chemical potential of the adsorbed silver. At 0 K, this is a straightforward task since the coverage-dependent chemical potential can be determined directly by computing the derivative of the convex hull of the binding energy data. The equilibrium surface coverage can then be obtained for a range of electrode potentials through the equilibrium condition defined by Eq. 43. As shown in Fig. 10b, if we consider the 0 μF/cm^2 case, the silver monolayer is predicted to desorb in a single step at an electrode potential of 0.78 V versus the SHE. This is inline with what was found with the binding energy data since the only ground states present were the clean and fully covered surface. Alternatively, for the 30 μF/cm^2 case, we find that the silver monolayer is predicted to desorb over the course of several steps as suggested by the higher number of ground states present on the voltage-sensitive convex hulls. While it is useful to consider 0 K results to gain a general understanding of adsorption trends, it is considerably more interesting to study adsorption behavior at room temperature since experiments are usually carried out under ambient conditions. This can be achieved by employing a force field or an analogous model that can be trained to predict the binding energies determined from quantum-continuum calculations. In this example, we have employed a *cluster expansion* approach that models configuration-dependent quantities as a series expansion of interacting sites or *clusters* on a lattice.[26, 15] Using the cluster expansion approximation for the electrochemical enthalpies, grand canonical Monte Carlo simulations can be performed to rapidly sample the configurational space and to subsequently estimate the average surface coverage at a fixed ion chemical potential, temperature, and electrode potential. In these simulations, a lattice of adsorption sites is modeled to be in contact with a reservoir of silver ions, along with a potentiostat and a thermostat that the system can exchange silver atoms, electronic charge, and thermal energy with. A trajectory is generated by randomly proposing new configurations through a series of trial moves and accepting or rejecting them according to the criteria set forth by the *Metropolis algorithm*.[27, 19] A trial move would consist of selecting a lattice site at random and adding (removing) a silver atom if the site is empty (occupied). The electrochemical enthalpy of the newly proposed configuration is computed, which is then used to compute the relative Boltzmann probability of the proposed configuration (P_p) to the current configuration (P_c)

$$\frac{P_p}{P_c} = \frac{\exp[-\beta(F_p - N_p\mu_{\mathrm{Ag}^+ + e^-})]}{\exp[-\beta(F_c - N_c\mu_{\mathrm{Ag}^+ + e^-})]} = \exp[-\beta(\Delta F - \Delta N\mu_{\mathrm{Ag}^+ + e^-})], \tag{46}$$

where $\mu_{\mathrm{Ag}^+ + e^-} = \mu_{\mathrm{Ag}^+} - e_0\Phi$ is the coupled chemical potential of the silver ions in solution and electrons in the electrode. The trajectory is updated at each step of the simulation by drawing a random number from a uniform probability distribution over the range $[0, 1]$. If the random number is less than or equal to the probability ratio, the newly proposed configuration is accepted and added to the trajectory as the next configuration; otherwise, the proposed configuration is rejected and the current configuration is added in its place.[10] The average coverage can then be computed as

$$\langle\theta\rangle = \frac{1}{N}\sum_{i=1}^{N}\theta_i, \tag{47}$$

where N is the number of steps over which the average is being computed, and θ_i is the coverage of configuration i in the trajectory. The adsorption isotherms for the 0 and 30 μF/cm^2 cases computed at 298 K are plotted on top of the 0 K isotherms in Fig. 10b. Here we observe that at finite temperature, the 0 μF/cm^2 isotherm still predicts the monolayer to desorb in a single step, while several of the predicted steps in the 30 μF/cm^2 case have been smoothed to reveal an overall two step desorption process. The finite capacitance case is more closely aligned with the experimental voltammetry which revealed a three step desorption

[10] It is crucial in the event of a rejection to recycle the previous configuration to ensure the configurations are sampled according to the Boltzmann distribution.[27, 19]

process. While the first two peak positions of the voltammetry are predicted fairly well with this model, we find that the presence of the third peak cannot be attributed to surface charge effects alone. A likely explanation for this may be found in Fig. 9, where we observe that the potential of zero charge of the gold (100) surface with low silver surface coverage is predicted to be less than 0.4 V versus the SHE. Therefore, at electrode potentials positive of this, the silver-covered surface is predicted to have a net positive charge. The presence of a positive surface charge would provide a driving force for the co-adsorption of anions such as the bisulfate or sulfate anions present in the electrolyte. Although this is a feature that has not been presently considered in this example, it is highly anticipated to improve the agreement of the predictions with voltammetric results.

Acknowledgements

A portion of this work was performed under the auspices of the U.S. Department of Energy by Lawrence Livermore National Laboratory under Contract DE-AC52-07NA27344. I.D. acknowledges financial support from the U.S. Department of Energy, Office of Science, Basic Energy Sciences, CPIMS Program, under Award No. DE-SC0018646.

References

[1] J. Greeley, I. Stephens, A. Bondarenko, T. P. Johansson, H. A. Hansen, T. Jaramillo, J. Rossmeisl, I. Chorkendorff, and J. K. Nørskov, "Alloys of platinum and early transition metals as oxygen reduction electrocatalysts," *Nature chemistry*, vol. 1, no. 7, p. 552, 2009.

[2] Z. W. Seh, J. Kibsgaard, C. F. Dickens, I. Chorkendorff, J. K. Nørskov, and T. F. Jaramillo, "Combining theory and experiment in electrocatalysis: Insights into materials design," *Science*, vol. 355, no. 6321, p. eaad4998, 2017.

[3] B. E. Hayden, "Particle size and support effects in electrocatalysis," *Accounts of chemical research*, vol. 46, no. 8, pp. 1858–1866, 2013.

[4] L. Li, A. H. Larsen, N. A. Romero, V. A. Morozov, C. Glinsvad, F. Abild-Pedersen, J. Greeley, K. W. Jacobsen, and J. K. Nørskov, "Investigation of catalytic finite-size-effects of platinum metal clusters," *The journal of physical chemistry letters*, vol. 4, no. 1, pp. 222–226, 2012.

[5] P. Liu and J. K. Nørskov, "Ligand and ensemble effects in adsorption on alloy surfaces," *Physical Chemistry Chemical Physics*, vol. 3, no. 17, pp. 3814–3818, 2001.

[6] M. Mavrikakis, B. Hammer, and J. K. Nørskov, "Effect of strain on the reactivity of metal surfaces," *Physical Review Letters*, vol. 81, no. 13, p. 2819, 1998.

[7] D. A. Slanac, W. G. Hardin, K. P. Johnston, and K. J. Stevenson, "Atomic ensemble and electronic effects in ag-rich agpd nanoalloy catalysts for oxygen reduction in alkaline media," *Journal of the American Chemical Society*, vol. 134, no. 23, pp. 9812–9819, 2012.

[8] M. Watanabe and S. Motoo, "Electrocatalysis by ad-atoms: Part iii. enhancement of the oxidation of carbon monoxide on platinum by ruthenium ad-atoms," *Journal of Electroanalytical Chemistry and Interfacial Electrochemistry*, vol. 60, no. 3, pp. 275–283, 1975.

[9] J. Greeley and M. Mavrikakis, "Alloy catalysts designed from first principles," *Nature materials*, vol. 3, no. 11, p. 810, 2004.

[10] J. Greeley, T. F. Jaramillo, J. Bonde, I. Chorkendorff, and J. K. Nørskov, "Computational high-throughput screening of electrocatalytic materials for hydrogen evolution," in *Materials For Sustainable Energy: A Collection of Peer-Reviewed Research and Review Articles from Nature Publishing Group*, pp. 280–284, World Scientific, 2011.

[11] Y.-T. Kim, P. P. Lopes, S.-A. Park, A.-Y. Lee, J. Lim, H. Lee, S. Back, Y. Jung, N. Danilovic, V. Stamenkovic, *et al.*, "Balancing activity, stability and conductivity of nanoporous core-shell iridium/iridium oxide oxygen evolution catalysts," *Nature Communications*, vol. 8, no. 1, p. 1449, 2017.

[12] H. B. Callen, "Thermodynamics and an introduction to thermostatistics," 1985.

[13] D. Chandler, "Introduction to modern statistical mechanics," 1987.

[14] S. E. Weitzner and I. Dabo, "Voltage effects on the stability of pd ensembles in pd–au/au (111) surface alloys," *The Journal of Chemical Physics*, vol. 150, no. 4, p. 041715, 2019.

[15] S. E. Weitzner and I. Dabo, "Voltage-dependent cluster expansion for electrified solid-liquid interfaces: Application to the electrochemical deposition of transition metals," *Physical Review B*, vol. 96, no. 20, p. 205134, 2017.

[16] A. Warshel, M. Kato, and A. V. Pisliakov, "Polarizable force fields: history, test cases, and prospects," *Journal of Chemical Theory and Computation*, vol. 3, no. 6, pp. 2034–2045, 2007.

[17] J. Yu, S. B. Sinnott, and S. R. Phillpot, "Charge optimized many-body potential for the si/ sio 2 system," *Physical Review B*, vol. 75, no. 8, p. 085311, 2007.

[18] A. C. Van Duin, S. Dasgupta, F. Lorant, and W. A. Goddard, "Reaxff: a reactive force field for hydrocarbons," *The Journal of Physical Chemistry A*, vol. 105, no. 41, pp. 9396–9409, 2001.

[19] D. P. Landau and K. Binder, *A guide to Monte Carlo simulations in statistical physics*. Cambridge university press, 2014.

[20] A. J. Bard, L. R. Faulkner, J. Leddy, and C. G. Zoski, *Electrochemical methods: fundamentals and applications*, vol. 2. wiley New York, 1980.

[21] S. Trasatti, "The absolute electrode potential: an explanatory note (recommendations 1986)," *Pure and Applied Chemistry*, vol. 58, no. 7, pp. 955–966, 1986.

[22] S. E. Weitzner and I. Dabo, "Quantum–continuum simulation of underpotential deposition at electrified metal–solution interfaces," *npj Computational Materials*, vol. 3, no. 1, p. 1, 2017.

[23] O. Andreussi, I. Dabo, and N. Marzari, "Revised self-consistent continuum solvation in electronic-structure calculations," *The Journal of chemical physics*, vol. 136, no. 6, p. 064102, 2012.

[24] P. Giannozzi, S. Baroni, N. Bonini, M. Calandra, R. Car, C. Cavazzoni, D. Ceresoli, G. L. Chiarotti, M. Cococcioni, I. Dabo, *et al.*, "Quantum espresso: a modular and open-source software project for quantum simulations of materials," *Journal of physics: Condensed matter*, vol. 21, no. 39, p. 395502, 2009.

[25] S. Garcia, D. Salinas, C. Mayer, E. Schmidt, G. Staikov, and W. Lorenz, "Ag upd on au (100) and au (111)," *Electrochimica acta*, vol. 43, no. 19-20, pp. 3007–3019, 1998.

[26] J. M. Sanchez, F. Ducastelle, and D. Gratias, "Generalized cluster description of multicomponent systems," *Physica A: Statistical Mechanics and its Applications*, vol. 128, no. 1-2, pp. 334–350, 1984.

[27] N. Metropolis, A. W. Rosenbluth, M. N. Rosenbluth, A. H. Teller, and E. Teller, "Equation of state calculations by fast computing machines," *The journal of chemical physics*, vol. 21, no. 6, pp. 1087–1092, 1953.